Applied Catalysis B: Environmental 84 (2008) 106–111

Contents lists available at ScienceDirect

Applied Catalysis B: Environmental

journal homepage: www.elsevier.com/locate/apcatb

Cobalt catalysts promoted with cerium and lanthanum applied to partial oxidation of methane reactions

Alessandra F. Lucrédio [a], Gregory Jerkiewicz [b], Elisabete M. Assaf [a,*]

[a] Instituto de Química de São Carlos, Universidade de São Paulo, Av. Trabalhador São Carlense, 400 São Carlos, SP 13560-970, Brazil
[b] Department of Chemistry, Queen's University, 90 Bader Lane, Kingston, ON K7L3N6, Canada

ARTICLE INFO

Article history:
Received 10 October 2007
Received in revised form 21 February 2008
Accepted 13 March 2008
Available online 21 March 2008

Keywords:
Hydrotalcite
Cobalt
Promoter
Methane partial oxidation

ABSTRACT

Catalysts of Co/Mg/Al promoted with Ce and La were tested in the catalytic partial oxidation of methane (POM) reaction. The addition of promoters was made by anion-exchange. X-ray diffraction (XRD) confirmed the formation of hydrotalcite phase for precursors. The mixed oxides were characterized as a mixture of Co_3O_4, periclase (Co, Al)MgO and/or spinel structure (Mg, Co)Al_2O_4. In the catalytic POM reaction over the promoted catalysts, a reduction in the carbon formation rate was found.

1. Introduction

In the last years, the conversion of natural gas – whose main component is methane – into chemical products with higher aggregated value and applicability has been one of the most important catalysis fields. Besides natural gas, another growing source of methane is biogas, generated as a sub-product in the anaerobic treatment of waste water [1]. This treatment presents a great environmental impact due to the removal of the organic matter from waste water and to the fact that the biogas generated can be converted into energy. One of the principal applications of methane is synthesis gas (syngas) production. Syngas, a mixture of H_2 and CO, is widely used as intermediary in the chemical process industry, such as methanol and ammonium production and Fischer–Tropsch process.

The partial oxidation of methane (POM), reaction (1), is a reaction that leads to a molar ratio of H_2:CO = 2:1 suitable for syngas generation.

$$CH_4 + \tfrac{1}{2}O_2 \rightarrow CO + 2H_2, \quad \Delta H^{\circ}_{298\,K} = -35.5\ \text{kJ mol}^{-1} \tag{1}$$

This reaction is mildly exothermic; however a small decrease for CO selectivity could lead to the formation of hot spots, with catalyst destruction [2]. It has been shown that catalysts obtained from hydrotalcite-type precursors are coking resistant [3,4] and have potential to minimize the difficulties inherent to the POM process: high temperatures and catalyst deactivation.

The reaction pathway can also include parallel reactions such as total catalytic combustion of methane and reforming of the remaining methane with steam or carbon dioxide, reactions (2), (3) and (4), respectively [5].

$$CH_4 + 2O_2 \rightarrow CO_2 + 2H_2O, \quad \Delta H^{\circ}_{298\,K} = -801.7\ \text{kJ mol}^{-1} \tag{2}$$

$$CH_4 + H_2O \rightarrow CO + 3H_2, \quad \Delta H^{\circ}_{298\,K} = +206\ \text{kJ mol}^{-1} \tag{3}$$

$$CH_4 + CO_2 \rightarrow 2CO + 2H_2, \quad \Delta H^{\circ}_{298\,K} = +247.5\ \text{kJ mol}^{-1} \tag{4}$$

Basile et al. [5] studied Ni/Mg/Al catalysts derived from hydrotalcites, prepared by thermal treatment at 900 °C, in POM, and observed that catalysts with low nickel content needed severe reduction treatment due to the formation of the solid solution of NiO–MgO, which presented high activity for the reaction. The catalysts with higher nickel content needed mild conditions for activation, but deactivated due to carbon formation. X-ray diffraction (XRD) and temperature-programmed reduction (TPR) analysis showed the presence of the NiO and (Ni, Mg)Al_2O_3 phases for these catalysts.

Choudhary and Mamman [6] compared the behavior of the solid solutions CoO–MgO and NiO–MgO in POM at 700 °C and showed an inferior performance of Co catalysts to Ni catalysts when compared at molar ratio of CH_4:O_2 = 2:1, however when

* Corresponding author.
E-mail address: eassaf@iqsc.usp.br (E.M. Assaf).

0926-3373/$ – see front matter © 2008 Elsevier B.V. All rights reserved.
doi:10.1016/j.apcatb.2008.03.008

compared at molar ratio of CH_4:O_2 = 4:1 the catalysts presented similar results.

Lucrédio and Assaf [4] studied the application of cobalt catalysts prepared by hydrotalcite-type precursors of Mg, Al and Co in the methane steam reforming and showed that these catalysts presented activity and selectivity for H_2 and CO with low carbon formation in 30 h of reaction.

According to the literature, the utilization of cerium and lanthanum as promoters of Ni/Al_2O_3 catalysts in dry reforming of methane increased the thermal stability, resistance to carbon formation and catalytic activity [7].

The addition of small quantities of rare earth oxides, which have basic properties, to the structure of hydrotalcite, can change the hydrotalcites characteristics after thermal treatment by the increasing of hydrotalcites basicity [8].

The structure of the anionic clays, as shown below, presents good anion-exchange capacity, and the interlamelar space can be used to introduce cations with high cationic radius values, which are not compatible with the octahedral sites of brucite sheets, such as Ce and La, in the anionic complexes form [9].

$$[M_{1-x}^{2+}M_x^{3+}(OH)_2]^{x+}[A_{x/n}]^{n-}\cdot mH_2O$$

Considering those aspects, the goal of this paper is to study the effect of the addition of promoters Ce and La in Co/Mg/Al catalysts, prepared from hydrotalcite-type precursors, in POM reactions to evaluate the products distribution and velocity of carbon formation.

2. Experimental

2.1. Synthesis

The unpromoted catalyst's precursor CoMgAl hydrotalcite-type (Ht) was prepared by the traditional technique of precipitation with carbonate. The promoted catalysts' precursors were prepared from Mg/Al/Co hydrotalcite obtained by precipitation with NaOH, which owns higher anion-exchange capacity than carbonate. This hydrotalcite was submitted to anion-exchange process with chelate type complexes of La and Ce for introduction of these cations into the CoMgAl-Ht, using the fact that Ce^{3+} and La^{3+} can react with the anionic chelating agent $EDTA^{-4}$, making the highly stable complex $[Me(EDTA)]^{-1}$.The conditions used in the precipitations were 65 °C of temperature and pH 10 controlled by NaOH 1 M addition.

(A) *Traditional method of precipitation* (Tr–Co): prepared by dropwise addition of an aqueous solution (100 mL) containing Co(II), Mg(II) and Al(III) nitrates (5, 25 and 10 mmol) to a continually stirred solution of sodium carbonate (30 mmol in 200 mL). The resulting suspension was stirred at 65 °C for 1 h. Next, the precipitate was aged at the same temperature for 18 h without stirring. The precipitate was separated by filtration, rinsed with deionized water, dried in air at 80 °C for 24 h and reserved.

The lanthanum and cerium introduction was made by anion-exchange method (Ae–La/Ce–Co) due to the high value of ionic radius of lanthanum and cerium when compared to magnesium, according to the method described by Fonseca and Assaf [3,4] and Tsyganok et al. [10]: a lanthanum/cerium chelate complex was utilized for the synthesis below. It was prepared by adding lanthanum/cerium(III) nitrate solution (50 mmol in 100 mL of water) to tetrasodium EDTA solution (50 mmol in 100 mL of water) at 65 °C. This solution was denominated $(Ce/LaY)^{-1}$.

(B) *Anion-exchange method* (Ae–MeCo): for this method, first the CoMgAl-Ht was obtained through the addition of Co(II), Mg(II) and Al(III) nitrates (5, 25 and 10 mmol dissolved in 100 mL of water) to 1 M aqueous NaOH solution, with stirring. The resulting suspension was stirred at 65 °C for 1 h. Next, the precipitate was aged at the same temperature for 18 h without stirring and then reserved.

Lanthanum/cerium chelate solution was added to this suspension. The suspension was stirred for 24 h at room temperature and the precipitate received the same treatment as described in (A).

The hydrotalcites were calcined at 500 °C in air for 15 h, and denominated Tr–Co–Calc., Ae–LaCo–Calc. and Ae–CeCo–Calc.

2.2. Characterization

The surface composition was determined by X-ray photoelectron spectroscopy (XPS) analysis. The XPS measurements were performed using a Thermo VG MICROLAB 310-F instrument. The data were collected with Mg Kα X-ray source using analyzer pass energy of 50 eV of energy. The calcined samples, mixed oxides, were used in form of pellets and fixed on a copper holder by copper tape. The charger was corrected using the C 1s peak.

The bulk composition was determined by energy-dispersive X-ray spectroscopy (EDS) analysis, using a scanning electron microscopy LEO 440 linked to an Oxford 7060 microanalyzer.

X-ray diffraction patterns were collected at room temperature in a URD-6 Carl Zeiss diffractometer with Cu Kα radiation (λ = 1.54056 Å). The spectra were scanned in the range 2θ = 3–80° at a step rate of 2 ° min^{-1}.

Specific surface area, average pore radius and total pore volume of mixture oxides were measured by adsorption of N_2 according to the method elaborated by Brunauer, Emmett and Teller (B.E.T.) using NOVA Data Analysis equipment.

Temperature-programmed reduction with hydrogen (H_2-TPR) of the catalysts was performed in Micromerits Chemisorb 2705 equipment, using 50 mg of catalyst and a temperature ramp from 25 to 1000 °C at 10 °C min^{-1}. A flow rate of the 30 mL min^{-1} of 5%H_2/N_2 was used.

2.3. Catalytic tests

The catalytic tests were performed in atmospheric pressure in a fixed-bed tubular quartz micro-reactor, in order to analyze the activity, product distribution and velocity of carbon formation as a function of reaction time. A specific apparatus was used and the analyses of the reactants and all the reaction products were carried out in-line by gas chromatograph (Varian, Model 3800) with two thermal conductivity detectors. The experimental methodology and the equipment used for these analyzes were previously described by the authors [11].

Prior to the reaction, 100 mg of the catalyst, sieved in the range of 60–100 mesh, right after the calcination process, were introduced into the reactor and reduced in situ in flowing of H_2 (50 mL min^{-1}) at 550 °C (10 °C min^{-1}) for 1 h, to activate the catalyst. Next, the sample was heated to 750 °C under a flow of pure N_2. The catalytic bed temperature was measured by the use of a thermocouple close to the reactor. The reaction was started in a hydrogen-free feed. The CH_4 flow was 40 mL min^{-1} and the feed molar ratio used was CH_4:O_2 = 2:1 and 4:1. Synthetic air was used like O_2 source. At the end of 24 h of catalytic test, the flow of CH_4:O_2 was stopped and the catalyst was cooled under a N_2 stream.

Table 1
Surface composition obtained by XPS and bulk composition obtained by EDS

Catalyst calcined	Molar composition (XPS)					Molar composition (EDS)				
	Co	Mg	Al	La	Ce	Co	Mg	Al	La	Ce
Tr–Co	0.11	0.67	0.22	–	–	0.07	0.67	0.26	–	–
Ae–LaCo	0.17	0.67	0.12	0.04	–	0.08	0.76	0.15	0.01	–
Ae–CeCo	0.17	0.60	0.19	–	0.04	0.08	0.75	0.15	–	0.02
Catalyst calcined	Massic composition (XPS)					Massic composition (EDS)				
	Co	Mg	Al	La	Ce	Co	Mg	Al	La	Ce
Tr–Co	0.22	0.57	0.21	–	–	0.14	0.60	0.26	–	–
Ae–LaCo	0.28	0.47	0.09	0.16	–	0.17	0.65	0.14	0.04	–
Ae–CeCo	0.29	0.42	0.15	–	0.14	0.17	0.60	0.13	–	0.10

The methane conversion and product yield were calculated by the following equations:

$$\text{Methane conversion}(X_{CH_4}): \quad \frac{\text{Mols. of } CH_4 \text{ converted}}{\text{Mols. of } CH_4 \text{ fed}} \tag{1}$$

$$\text{Product yield}(Y_i): \quad \frac{\text{Mols. of } i \text{ produced}}{\text{Mols. of } CH_4 \text{ converted}} \tag{2}$$

3. Results and discussion

Table 1 presents the surface compositions, molar composition and massic composition, obtained by XPS, and the bulk compositions, obtained by EDS. By comparing these results it is possible to observe that the values of Al^{3+} concentration are lower, for the promoted catalysts, than the values used in the precipitation (molar composition: $Co_{0.125}Mg_{0.625}Al_{0.25}$), which cause the differences on the *x* value (Table 2). The differences that are occurring in the *x* value for Ae–LaCo and Ae–CeCo catalysts may be occurring due to the method of preparation, where the loss of Al^{3+} is attributed to the formation of water-soluble aluminates reaction from aluminum hydroxide ($Al(OH)_3 + OH^- \rightleftarrows [Al(OH)_4]^-$) at moderately high pH and the long time, 24 h, used for the anion-exchange [4,12].

The higher Co concentration, Table 1, on the surface when compared with bulk results could be occurring by the formation of Co^{3+} species during the thermal treatment in air. These new species, Co^{3+}, claim the creation of additional charges to keep the structure neutrality, by the production of defects, like cationic vacancies type, which cause the cobalt cations migration to surface [13].

Also, for the promoted catalysts, the concentration of La and Ce was higher on the surface than in the bulk. These results could suggest that only part of these complexes was introduced in the interlayer of hydrotalcite and part of these complexes was deposited on the surface of the precursor. Along with this effect, the thermal treatment could have favored the migration of La and Ce cations to the surface, due to the high ionic radius, leading to the high content of La and Ce on the surface.

Table 2
x value, lattice parameters *a* and *c* and particle size

Sample	*x*[a]	*a* precursor (nm)	*c* precursor (nm)	*a* oxide (nm)	Particle size[b] (nm)
Tr–Co	0.26	0.305	2.264	0.415	3.4
Ae–LaCo	0.18	0.307	2.382	0.419	4.5
Ae–CeCo	0.17	0.307	2.391	0.418	6.3

[a] $x = M^{3+}/(M^{2+} + M^{3+})$ (values obtained by EDS analysis).
[b] Particle size for calcined sample calculated based on Scherrer equation, $D = K^*\lambda/\beta^*\cos(\theta)$ and using the most intense peak (200) located in $2\theta = 42.91^\circ$.

Fig. 1A presents the X-ray patterns of the precursors. According to this figure, it is possible to observe the formation of a hydrotalcite-type structure, which presents narrow and symmetric reflexions for (0 0 3), (0 0 6), (1 1 0) and (1 1 3) planes and wide and asymmetric reflexions for (1 0 2), (1 0 5) and (1 0 8) planes that are characteristics of lamellar compounds of rhombohedric symmetry [14,15]. Table 2 presents values of cell parameters *a* (calculated by the equation: $a = 2^*d(1\,1\,0)$) and *c* (calculated by the equation: $c = 3^*d(0\,0\,3)$) with higher values of *c* for the promoted samples than for the unpromoted ones. This happens due to an expansion caused by the introduction of chelate anion, which is bigger than hydroxyls and carbonates anions. Changes were not observed in the cell parameter *a*, which means

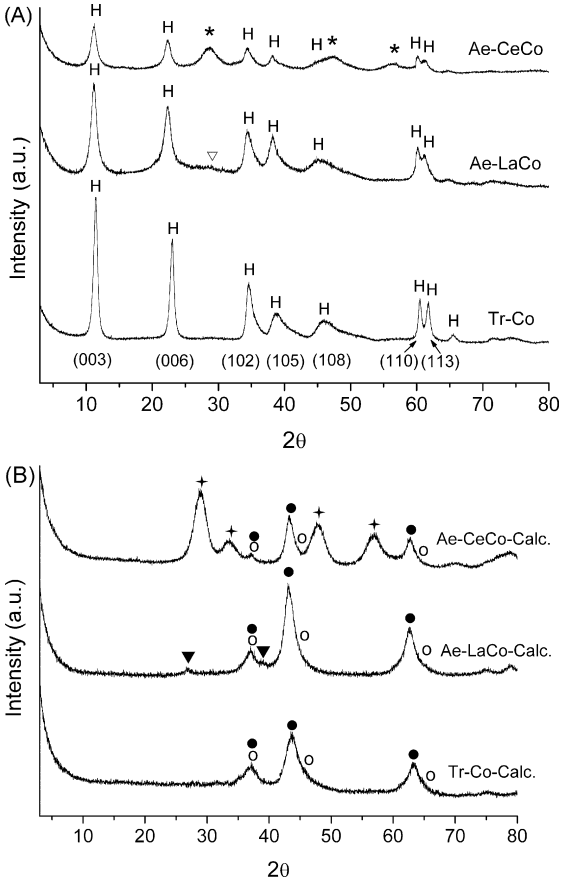

Fig. 1. X-ray patterns of (A) precursors (H: hydrotalcite, *: $Ce(OH)_3$, (▽) $La(OH)_3$) and (B) calcined samples ((●) MgO, CoO, (○) Co_3O_4 and/or $MgAl_2O_4$ and/or $CoAl_2O_4$ and/or $MgCo_2O_4$, (▼) La_2O_3, (+) Ce_2O_3 and/or CeO_2).

Table 3
Surface area, average pore radius and total pore volume

Catalyst	Surface area-B.E.T. ($m^2\,g^{-1}$)	Average pore radius (Å)	Total pore volume ($cm^3\,g^{-1}$)
Tr–Co	132	23.4	0.15
Ae–LaCo	116	52.8	0.31
Ae–CeCo	133	37.1	0.25

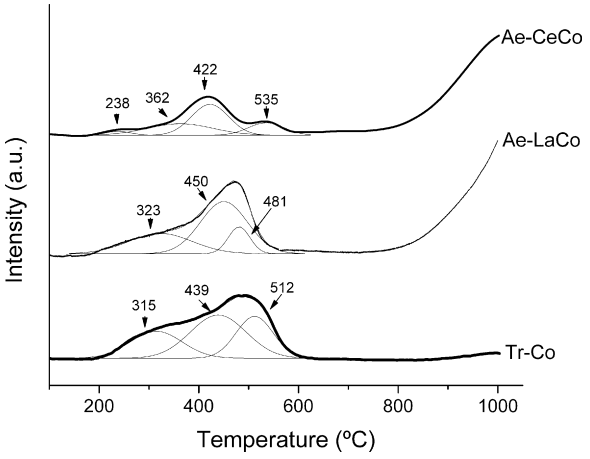

Fig. 2. TPR patterns of calcined samples.

that there were no changes to the average cation–cation distance in the brucite sheets, with promoter introduction. The Ae–LaCo and Ae–CeCo precursors also presented additional diffraction lines indicating an excess of La and Ce, in the form of $La(OH)_3$ and $Ce(OH)_3$ [16].

Fig. 1B presents the X-ray patterns of calcined samples. In the figure, it is possible to see the disappearing of the hydrotalcite-type structure and the appearing of new peaks referring to the oxide phases of Co, Mg and Al. Table 2 presents the values of cell parameter *a* of oxide phase (calculated by the most intense peak for CoO and MgO in $2\theta \sim 45^\circ$ referring to plane (4 4 0) of oxide phase). The cell parameter *a* values indicate values lower than the standard of CoO and MgO (*a*MgO = 0.421 nm and *a*CoO = 0.426 nm) [16], which could be an indicative of incorporation of Al^{3+} species ($r_{Al^{3+}} = 0.50$; $r_{Mg^{2+}} = 0.65$; $r_{Co^{2+/3+}} = 0.78/0.62$) of lower ionic radius. These results suggest that the mixed oxides could be in the form of periclase Mg(Co, Al)O and along with this phases could be present the spinel phase Co_3O_4 and (Mg, Co)Al_2O_4 and/or $MgCo_2O_4$. The samples promoted with La and Ce also presented peaks attributed to the oxide phases La_2O_3 and CeO_2/Ce_2O_3.

Table 3 presents the textural parameters of the calcined samples. The results show similar areas for samples Tr–Co and Ae–CeCo and a smaller area for Ae–LaCo, however the Tr–Co presents smaller pore radius and pore volume than Ae–LaCo and Ae–CeCo.

These observed differences could be occurring due to the preparation method that was used, where for Ae–LaCo and Ae–CeCo a chelate complex was used to introduce the cerium and lanthanum in the structure of hydrotalcite. With the thermal treatment, these complexes were decomposed in volatile species and liberated along with the H_2O and CO_2, which are usually observed for hydrotalcites prepared by traditional precipitation with carbonate. This effect could be the reason why the promoted samples are presenting higher pore radius and volume than Tr–Co sample and also could be an indication of the chelate introduction into the interlamelar space of hydrotalcite [17–20].

Fig. 2 presents the TPR patterns of calcined samples. The results show a region under 550 °C, which can be decomposed in three reducible phases. The region around 250 and 400 °C (Tr–Co = 315 and 440 °C; Ae–LaCo = 323 and 450 °C and Ae–CeCo = 238 and 362 °C), according to Khassin et al. [21], is referring to the reduction of Co_3O_4 species, which can occur in two steps forming CoO and Co^0, respectively. The region around 500 °C (Tr–Co = 512 °C; Ae–LaCo = 480 °C and Ae–CeCo = 422 °C) is attributed to the reduction of species $Co^{2+/3+}$ interacted in non-stoichiometric form with the oxide support of Mg and Al [18]. It could also be observed that the sample Ae–LaCo presented a

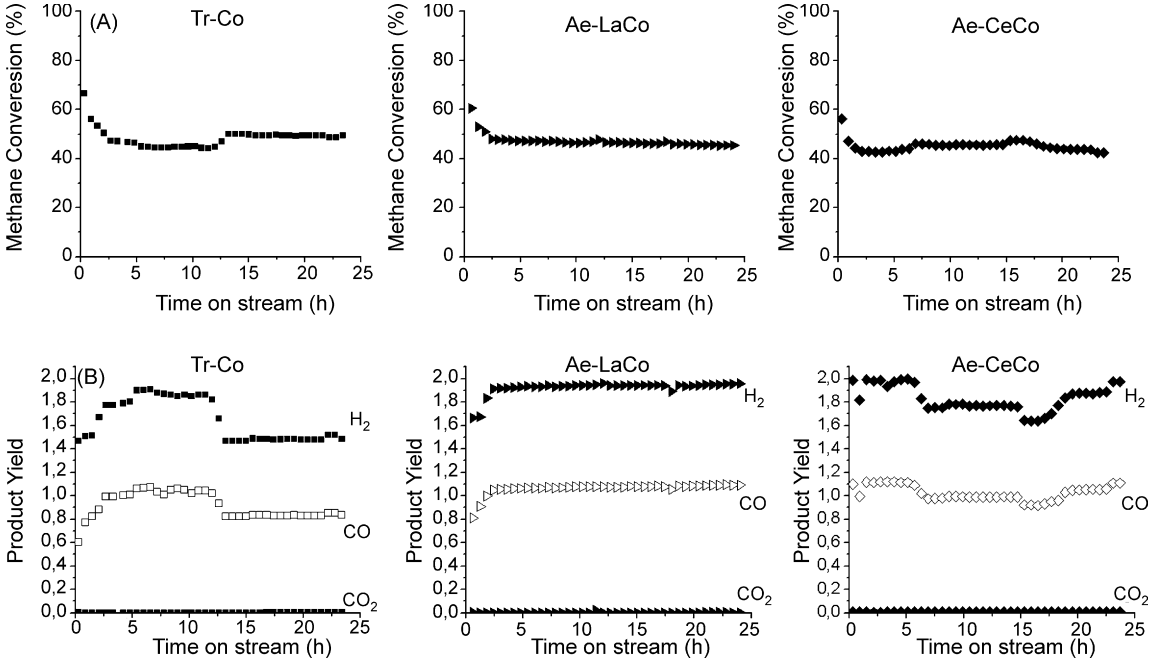

Fig. 3. (A) Methane conversion and (B) product yield (mol_i produced/mol_{CH_4} converted).

Table 4
Average values of methane conversion (%), H_2 yield, CO yield, CO_2 yield and rate of *C* formation (mmol min^{-1})

Catalyst	XCH_4 (%)	YH_2 (mol)	YCO (mol)	YCO_2 (mol)	C^a (mmol min^{-1})	C^b (mmol min^{-1})
Tr–Co	50	1.6	0.9	0.02	0.095	0.010
Ae–LaCo	47	1.9	1.0	0.02	–	0.003
Ae–CeCo	45	1.8	1.0	0.01	–	0.002

[a] C = molar flow $CH_{4\ in}$ − molar flow $(CH_4 + CO + CO_2)_{out}$.
[b] *C* = based on the difference between the mass of catalyst after the reaction and before the reaction.

pattern very similar to the one presented by the sample prepared by the traditional technique. However the peak referring to the reduction of Co species interacted in the form non-stoichiometric with the support appears in lower temperature, which can be an indication of lower interaction of these species with the support for this sample. The sample Ae–CeCo presented lower reduction temperature for all peaks, probably due to a small metal–support interaction. For this sample, it is still possible to see the reduction of an additional phase in 535 °C referring to superficial reduction of CeO_2 to Ce_2O_3 [7]. Samples Ae–LaCo and Ae–CeCo presented a peak started around 800 °C, which according to the XRD results, could be referring to the reduction of the periclase Mg(Al, Co)O and/or spinel (Mg, Co)Al_2O_4 phase. This peak is not observed for the Tr–Co sample in Fig. 2. It is possible that the reduction of these phases is occurring in higher temperatures due to the higher metal–support interaction presented for this sample. According to Table 2, the Tr–Co sample presented a smaller particle size than Ae–CeCo and Ae–LaCo and this could be related with dispersion. Samples with smaller particle size are more dispersed on the support and, in this way, have a better interaction with the support and get reduced at higher temperatures [13].

According to the catalytic tests, the catalysts were not active in POM with molar feed of CH_4:O_2 = 2:1. They presented fast deactivation by oxidation of active sites, probably due to the higher concentration of oxygen to have favored an increase of velocity of dissociative adsorption of oxygen (reaction (5)) compared to methane decomposition (reactions (6)–(9)) [22–24]. The authors observed the same behavior for nickel catalysts prepared and tested in the same conditions [11].

$$O_2 + 2* \rightarrow 2O* \quad (5)$$

$$CH_4 + 2* \rightarrow CH_3* + H* \quad (6)$$

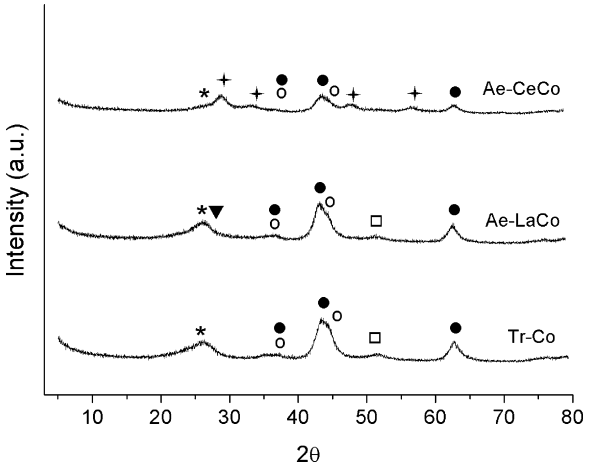

Fig. 4. X-ray patterns of the catalysts after 24 h of reaction ((●) MgO, CoO; (○) Co_3O_4 and/or $MgAl_2O_4$ and/or $CoAl_2O_4$ and/or $MgCo_2O_4$; (▼) La_2O_3; (+) Ce_2O_3 and/or CeO_2; (*) C; (□) Co^0).

$$CH_3* + * \rightarrow CH_2* + H* \quad (7)$$

$$CH_2* + * \rightarrow CH* + H* \quad (8)$$

$$CH* + * \rightarrow C* + H* \quad (9)$$

Fig. 3 presents the reactions with molar feed of CH_4:O_2 = 4:1, where it is possible to note that all catalysts presented average conversion around 50%. However, in the first hour of reaction, the catalysts presented initial conversions higher than 50%. This result can be explained by an excess of CH_4 decomposition (reactions (6)–(9)), compared to dissociative adsorption of oxygen (reaction (5)), leading to a carbon formation, as confirmed by carbon balance. However, after 1 h of reaction, the catalysts reached the equilibrium around 50% of conversion and kept this activity up to the end of 24 h, when the reaction was stopped. According to Table 4, the Tr–Co catalyst presented an average conversion of methane slightly higher than Ae–LaCo and Ae–CeCo, what can be associated with the decomposition of methane in carbon, according to the high rate of *C* formation observed for this catalyst.

In Fig. 3B and Table 4 it is possible to see that the addition of promoters led to a higher selectivity to CO formation than the unpromoted catalyst. This higher selectivity to CO is associated with a reduction of the carbon formation rate, indicating a favoring of the reaction between carbon and oxygen (reaction (10)) adsorbed on the surface. This is an indication that the addition of promoters favored the dissociative adsorption of the oxygen (reaction (5)) in these catalysts. This effect also can be associated to the high content of Ce and La on the surface, as observed by XPS results, and which can contribute for the increase of the surface basicity with consequent carbon reduction [25,26].

$$C* + O* \rightleftarrows CO* + * \quad (10)$$

These results are similar to those observed for nickel catalysts prepared in the same conditions by the authors [11].

Fig. 4 presents the XRD of catalysts after 24 h of reaction. According to Fig. 4, it is possible to observe that the hydrotalcite-phase was not regenerated and peaks related to MgO/CoO, La_2O_3, CeO_2/Ce_3O_4 and spinel phase are still present. Besides the cited peaks, it is also possible to observe the appearance of new peaks, in 2θ = 26.1 related to the presence of carbon species and around 2θ = 51.5 that could be related to remaining Co^0 [16].

For comparison, one sample of 18% Co/$MgAl_2O_4$ [27] prepared by impregnation method, which is usually used for preparation of commercial catalysts, was tested in POM reaction with molar feed of CH_4:O_2 = 4:1. The catalyst presented a conversion around 64%, with lower H_2 and CO yield (H_2 = 1.4; CO = 0.7 and CO_2 = 0.03) and higher rate of *C* formation (0.3 mmol min^{-1}) than the results obtained for catalysts derived from hydrotalcites (Table 4). The catalyst did not show stability for this reaction and deactivated after 3 h of reaction due to the high pressure into the reactor that occurred by the high concentration of carbon species on the catalytic bed.

4. Conclusions

The catalysts prepared from hydrotalcite-type precursors and promoted with Ce and La presented good performance in POM with feed molar ratio of CH_4:O_2 = 4:1 with similar conversions. The addition of promoters benefited the performance of catalysts by increasing the CO selectivity and decreasing the rate of C formation, possibly due to a favoring of reactions of adsorption and decomposition of oxygen on these promoted catalysts, which favored the gasification of carbon species.

Acknowledgements

The authors are grateful to the Brazilian federal research funding council, CNPq, CAPES and FAPESP for financial support and to the Department of Chemical Engineering at the Federal University of São Carlos for TPR and B.E.T. analysis.

References

[1] A. Noyola, J.M. Morgan-Sagastume, J. Lópes-Hernández, Rev. Environ. Sci. Biotechnol. 5 (2006) 93–114.
[2] E. Ruckenstein, Y.H. Hu, Appl. Catal. A 183 (1999) 85–92.
[3] A. Fonseca, E.M. Assaf, J. Power Sources 142 (2005) 154–159.
[4] A.F. Lucrédio, E.M. Assaf, J. Power Sources 159 (2006) 667–672.
[5] F. Basile, L. Basini, M.D. Amore, G. Fornasari, A. Guarinoni, D. Matteuzzi, G. Del Piero, F. Trifirò, A. Vaccari, J. Catal. 173 (1998) 247–256.
[6] V.R. Choudhary, A.S. Mamman, J. Chem. Technol. Biotechnol. 73 (1998) 345–350.
[7] L. Znak, K. Stolecki, J. Zielinski, Catal. Today 101 (2005) 65–71.
[8] E. Angelescu, O.D. Pavel, M. Che, R. Birjega, G. Constentin, Catal. Commun. 5 (2004) 647–651.
[9] A. Vaccari, Catal. Today 41 (1998) 53–71.
[10] A.I. Tsyganok, K. Suzuki, S. Hamakawa, K. Takehira, T. Hayakawa, Catal. Lett. 77 (2001) 75–86.
[11] A.F. Lucrédio, G. Jerkiewicz, E.M. Assaf, Appl. Catal. A 333 (2007) 90–95.
[12] A.I. Vogel, Química analítica qualitativa, Mestre Jou, São Paulo, 1981.
[13] A.R. West, Solid State Chemistry and its Applications, John Wiley, New York, 1984
[14] S. Casenave, H. Martinez, C. Guimon, A. Auroux, V. Hulea, A. Cordoneanu, E. Dumitru, Thermochim. Acta 379 (2001) 85–93.
[15] J. Pérez-Ramírez, G. Mul, J.A. Moulijn, Vib. Spectrosc. 27 (2001) 75–88.
[16] JCPDS – Joint Committee on Powder Diffraction Standards, International Center of Diffraction Data, Pennsylania, USA, 1994 (CD-ROM).
[17] R. Ciola, Fundamentos de Catálise, Editora da Universidade de São Paulo, São Paulo, 1981.
[18] L. Chmielarz, P. Kustrowski, A. Rafalka-Łasocha, R. Dziembaj, Thermochim. Acta 395 (2003) 225–236.
[19] D.G. Cantrell, L.J. Gillie, A.F. Lee, K. Wilson, Appl. Catal. A 287 (2005) 183–190.
[20] A. Tsyganok, A. Sayari, J. Solid State Chem. 179 (2006) 1830–1841.
[21] A.A. Khassin, T.M. Yurieva, V.V. Kaichev, V.I. Burkhtiyarov, A.A. Budneva, E.A. Paukshtis, V.N. Parmon, J. Mol. Catal. A: Chem. 175 (2001) 189–204.
[22] X. Zhang, C.S.M. Lee, D.O. Hayward, D.M.P. Mingos, Catal. Today 105 (2005) 283–294.
[23] J. Wei, E. Iglesia, J. Catal. 224 (2004) 370–383.
[24] J. Wei, E. Iglesia, J. Catal. 225 (2004) 116–127.
[25] A.S. Ivanova, B.L. Moroz, E.M. Moroz, Yu.V. Larichev, E.A. Paukshtis, V.I. Bukhtiyarovgg, J. Solid State Chem. 178 (2005) 3265–3274.
[26] D.L. Trimm, Catal. Today 49 (1999) 3–10.
[27] L.P.R. Profeti, E.A. Ticianelli, E.M. Assaf, Fuel 87 (2008) 2076–2081.